# Analyzing Unsteady Turbomachinery Flow Simulations with Mixing Entropy

**Christian Frey***
Institute of Propulsion Technology
German Aerospace Center (DLR)
Linder Höhe, 51147 Cologne
Germany
Email: christian.frey@dlr.de

**Benedict Geihe**
Institute of Propulsion Technology
German Aerospace Center (DLR)
Linder Höhe, 51147 Cologne
Germany
Current affiliation: Department
of Mathematics and Computer Science
University of Cologne
Germany

**Laura Junge**
Institute of Propulsion Technology
German Aerospace Center (DLR)
Linder Höhe, 51147 Cologne
Germany
Current affiliation: Leybold GmbH (Part of the Atlas Copco Group), Germany

## ABSTRACT

*The prediction of unsteady aerodynamic loads is a central problem during the design of turbomachinery. Over the last 20 years, harmonic balance methods have been shown to be highly efficient for this task. A CPU-cost optimal setup of a harmonic balance simulation, however, requires the knowledge about relevant harmonics. In the case of a single blade row with a periodic disturbance this question amounts to the classical problem of harmonic convergence, a problem which is solely due to the nonlinearity of the unsteady flow physics. In contrast, for multi-stage configurations, the choice of harmonics is further complicated by the fact that the interactions of disturbances with blade rows may give rise to a vast spectrum of harmonics that possibly have important modal content, e.g. Tyler-Sofrin*

*Address all correspondence to this author.

*modes.*

*The aim of this paper is to show that the mixing entropy attributed to circumferential modes of a given harmonic can serve as a disturbance metric on the basis of which a criterion could be derived whether a certain harmonic should be included or not. The idea is based on the observation that the entropy due to the temporal and circumferential mixing of the flow at a blade row interface may be decomposed, up to third-order terms, into independent contributions from different frequencies and mode orders. For a given harmonic balance (and steady) flow result, the mixing entropy attributed to modes which are simply mixed out, rather than resolved in the neighboring row, is shown to be a natural indicator of a potential inaccuracy.*

*We present important features of the mixing entropy for unsteady disturbances, in particular a close relationship to sound power for acoustic modes. The problem of mode selection in a 1.5-stage compressor configuration serves as a practical example to illustrate our findings.*

## INTRODUCTION

Unsteady aerodynamic loads can cause blade failure and must therefore be estimated during the design process. The most important causes for high-cycle fatigue are flutter and forced response. These are typically predicted by a URANS approach in the time- or frequency domain, most notably the harmonic balance method. Harmonic balance approaches, however, require the knowledge of relevant harmonics. In the case of a single blade row with a periodic disturbance this question amounts to that of harmonic convergence. In practice, a standard approach is similar to that of mesh refinement studies. One compares the results of a small number of setups with increasing number of harmonics until the results show an insignificant sensitivity to the inclusion of further harmonics.

In multi-blade row configurations, however, interactions of disturbances with neighboring blade rows may give rise to a vast spectrum of harmonics that can have important modal content, cf. [1, 2, 3] for blade row interactions and [4, 5, 6] for aerodynamic damping predictions. Observe that

the issue of selecting harmonics in multi-stage configurations is a problem which does not depend on strong nonlinearities. It would arise as well if, for instance, the modelling approach were based on the linearized Euler equations.

The generalization of the harmonic balance approach to include harmonics which are not simply integer multiples of some fundamental harmonic, is itself a delicate, but central issue in turbomachinery applications; whenever the unsteady flow due to both the up- and downstream neighbors is to be considered simultaneously, and the greatest common divisor of the neighboring blade counts is small (it is often equal to $1$), then the standard harmonic balance approach would be to take the shaft speed as fundamental angular frequency. Then, however, the harmonic balance approach loses much of its appeal, since the number of sampling points increases significantly. Moreover, stator-stator (or rotor-rotor) interactions give rise to harmonics which have integer multiples of the blade (or vane) passing frequencies but not a single interblade phase angle [7]. More precisely, the unsteady flows in the different passages can differ significantly. Note that this is in stark contrast to configurations of two blade rows, where the flows in the different passages are identical up to a certain phase shift. Over the last ten years, several authors (see, e.g., [8, 9, 10, 11, 12]) have adapted the original harmonic balance approach to tackle the above problems. The intricacies of the different extensions to multiple fundamental frequencies are, however, not the subject of this article.

The aim of this work is to show that the mixing entropy attributed to circumferential modes of a given harmonic can serve as a disturbance metric on the basis of which a criterion could be derived whether a certain harmonic should be included or not. The idea to use mixing entropy in the context of frequency-domain simulations is based on the fundamental observation by Fritsch and Giles [13, 14] that its second-order approximation decomposes into contributions from different frequencies and mode orders. Moreover, for each frequency and mode order, the contribution can be further decomposed into contributions from different wave types. Schlüß and Frey [15] gave a more insightful interpretation of the resulting formula by relating it to the waves' group velocities and a certain norm, whose square is defined by the Hessian of the entropy density. This way, Fritsch and Giles' main result could be shown to hold in much more general contexts, e.g., for

imperfect gas or multicomponent flow. In a recent paper, Frey et al. [16] have shown that the essential difference between a number of turbomachinery averaging techniques (entropy, work and flux average) is the amount of mixing entropy that the averagings attribute to certain mode types. In contrast, the notion of mixing entropy is shown in this paper to be useful to analyze periodic unsteady flows.

The article is organized as follows. We first introduce the harmonic balance approach adopted in this paper. Then basic properties of the mixing entropy of temporal and circumferential disturbances are derived. In particular, a close relationship to sound power will be established. Finally, we apply the harmonic balance method to a configuration comprising the first stator and the second stage of DLR's Rig 250. We focus on the first blade-passing frequency in the stator and compare a simulation with 3 harmonics that only resolves the influence of the up- and downstream neighboring rows with one that includes all Tyler-Sofrin modes using an appropriate multi-passage configuration. It is then shown how the presence of scattered harmonics can be anticipated well from the mixed-out disturbances at the rotor outlet in terms of their mixing entropy.

Finally, we compare the multi-passage simulation with a result based on harmonic sets, where each harmonic set captures the Tyler-Sofrin modes whose frequency is the first blade-passing frequency. The harmonic set approach is shown to yield almost identical results. Unlike the multi-passage configurations, however, it allows to add or omit modes in order to obtain a cost-efficient setup for a given problem. This underlines the relevance of physically meaningful quantities that serve as criteria for the inclusion of a particular harmonic.

## HARMONIC BALANCE

The harmonic balance (HB) solver employed is integrated into DLR's flow solver TRACE [10]. In the following, those features which are relevant for this paper are briefly sketched. The underlying spatial discretisation used in this paper is based on the finite volume approach with Roe's upwind scheme [17] for the inviscid numerical fluxes. MUSCL extrapolation [18] in combination with a van Albada type limiter [19] is used to achieve second order accuracy. Viscous fluxes are computed from second-order accurate central differences. For the simulation results presented

below, Wilcox' $k$-$\omega$ turbulence model [20] was used.

### Harmonic Set Approach

The Harmonic balance solver uses the concept of so-called *harmonic sets*. A harmonic set consists of a base angular frequency $\omega^0$, a base interblade phase angle $\sigma^0$ and a set of harmonic indices $k_1, \ldots, k_n$, where each harmonic index $k_j$ corresponds to a harmonic with angular frequency $k_j\omega^0$ and interblade phase angle $k_j\sigma^0$.

Formulated in the frequency domain, the HB method solves

$$\mathbf{i}\omega\widehat{q}_{(\omega,\sigma)} + \widehat{R(q)}_{(\omega,\sigma)} = 0, \tag{1}$$

for all harmonics $(\omega, \sigma)$. Here, the second term denotes the Fourier coefficient of the flow residual evaluated at an appropriate number of sampling points. For a single harmonic set with base angular frequency $\omega^0$ and equidistant sampling points

$$t_j = \frac{2\pi j}{\omega^0 N}, \quad j = 0, \ldots, N-1,$$

the second summand of (1) becomes the discrete Fourier transform. The number of sampling points $N$ is set to $N = (n_{\mathrm{hh}} - 1)k_{\max} + 1$ with $k_{\max}$ denoting the highest harmonic. $n_{\mathrm{hh}}$, the number of sampling points per period for the highest harmonic, must be at least $3$ in order to ensure that the highest harmonic is smaller or equal to the Nyquist frequency. $n_{\mathrm{hh}} = 4$ is the minimum value to guarantee that taking products of two harmonics does not result in a mode which is indistinguishable from some original harmonic, i.e., aliasing [21]. For the simulations below $n_{\mathrm{hh}} = 5$ has been used.

Consider now a general set $\mathscr{S}$ of harmonics and denote by $R^{\mathscr{S}}(t)$ the flow residual evaluated

at the reconstruction using only harmonics in $\mathscr{S}$, i.e.,

$$R^{\mathscr{S}}(t) = R\left(\mathrm{Re}\sum_{(\omega,\sigma)\in\mathscr{S}} \hat{q}_{(\omega,\sigma)} e^{\mathbf{i}\omega t}\right)$$

Then, denoting the $i$-th harmonic set by

$$\mathscr{S}_i = \{(k\omega_i^0, k\sigma_i^0) \,|\, k \in \mathscr{K}_i\}$$

the harmonic set approach is based on the following approximation

$$\begin{aligned} R^{\mathscr{S}_1\cup\mathscr{S}_2}(t) &= R^{\mathscr{S}_1}(t) + (R^{\mathscr{S}_2\cup\mathscr{S}_1}(t) - R^{\mathscr{S}_1}(t)) \\ &\approx R^{\mathscr{S}_1}(t) + (R^{\mathscr{S}_2}(t) - R^{\mathscr{S}_1\cap\mathscr{S}_2}(t)) \end{aligned} \tag{2}$$

for two harmonic sets $\mathscr{S}_1, \mathscr{S}_2$. In the last line of Eq. (2), all summands are time-periodic with base angular frequencies $\omega_i^0$ and base interblade phase angles $\sigma_i^0$. The third term, unless it consists of the zeroth harmonic only, is periodic as well, since $\mathscr{S}_1 \cap \mathscr{S}_2$ is again a harmonic set. Hence, one can apply discrete Fourier transforms efficiently to each of the terms to compute the Fourier coefficients. This idea can be generalized to include further harmonic sets. The approach applies to the case of several fundamental frequencies but also to cases with identical fundamental frequencies but different interblade phase angles. For more details, the reader is referred to [11].

**Mode Coupling and Solution Method**

The blade row coupling method used here, is based on a temporal and circumferential Fourier decomposition of the flow at the blade row interfaces

$$q = \mathrm{Re} \sum_{\omega,m} \left[ \hat{q}_{\omega,m} e^{\mathbf{i}(\omega t + m\theta)} \right] . \tag{3}$$

The mode matching condition for two modes $(\omega_i, m_i)$ in two rotational frames of references is

$$(\omega_1 + m_1(\Omega_2 - \Omega_1), m_1) = \pm(\omega_2, m_2) \tag{4}$$

where $\Omega_1, \Omega_2$ denote the rotational speeds. When the sign in Eq. (4) is negative, the complex conjugate of the Fourier coefficients has to be taken when transforming from one system to the other [22].

The blade row interface is integrated into the 2D-nonreflecting boundary condition. If, on the opposite side, no matching mode is found, then the local mode is treated exactly as in the non-reflecting boundary condition at inlets or outlets. Otherwise, the difference of local and remote amplitude is converged to zero, where each side drives the difference of incoming mode amplitudes to zero. When harmonics in some blade row are added to the HB configuration, the change in the results for the existing harmonics is thus due to the following:

- The truncation and aliasing errors in the blade row are reduced.
- Some modes at the row interfaces are now allowed to interact with neighboring blade rows, changing the result both in that blade row and, by reflection and transmission, possibly in the whole configuration.

Whereas the first phenomenon is related to the nonlinearity of the flow equations, the second aspect would have similar consequences for the problem of defining an HB setup if, for instance, the unsteady flow modelling were based on linearized equations.

## MIXING ENTROPY

In this section, we summarize the derivation of the asymptotic expansion of the mixing entropy presented in [15] and relate the result for acoustic modes to sound intensity. In the following, $\mathbf{D}F(q)$ denotes the Jacobian of a function $F$ in several variables $q_1, \ldots, q_n$. $\mathbf{D}F(q)[v]$ is thus the directional derivative in the direction of $v$. Taking a further directional derivative in the direction of $w$, say, results in

$$\mathbf{D}^2F(q)[v,w] = \sum_{i,j} \frac{\partial^2 F}{\partial q_i \partial q_j} v_i w_j.$$

By Schwarz's theorem, $\mathbf{D}^2F(q)$ is symmetric in $v$ and $w$. Taylor's theorem implies that for smooth $F$

$$F(q+v) = F(q) + \mathbf{D}F(q)[v] + \frac{1}{2}\mathbf{D}^2F(q)[v,v] + \mathrm{O}(\|v\|^3).$$

The Euler equations for a compressible fluid are a system of conservation laws,

$$\frac{\partial q}{\partial t} + \operatorname{div} F(q) = 0 \tag{5}$$

with $q$ being the conservative state vector $q = (\rho, \rho U, \rho e_\mathrm{t})$. One can rewrite Eq. (5) in terms of the flux Jacobians $\mathbf{D}F^x$ and $\mathbf{D}F^y$,

$$\frac{\partial q}{\partial t} + \mathbf{D}F^x(q)\frac{\partial q}{\partial x} + \mathbf{D}F^y(q)\frac{\partial q}{\partial y} = 0. \tag{6}$$

For any derived quantity $\varphi = \varphi(q)$ we have

$$\frac{\partial \varphi(q)}{\partial t} = \mathbf{D}\varphi(q)\frac{\partial q}{\partial t}.$$

So, Eq. (6) implies

$$\frac{\partial \varphi}{\partial t} + \mathbf{D}\varphi(q)\mathbf{D}F^x(q)\frac{\partial q}{\partial x} + \mathbf{D}\varphi(q)\mathbf{D}F^y(q)\frac{\partial q}{\partial y} = 0. \tag{7}$$

A scalar quantity $\varphi$ is called a generalized entropy if firstly it is strictly concave and secondly Eq. (7) can be written as a conservation law with an appropriate entropy flux $F_\varphi$,

$$\frac{\partial \varphi}{\partial t} + \operatorname{div} F_\varphi = 0. \tag{8}$$

This conservation law for $\varphi$ can be rewritten in terms of the entropy flux Jacobians,

$$\frac{\partial \varphi}{\partial t} + \mathbf{D}F^x_\varphi(q)\frac{\partial q}{\partial x} + \mathbf{D}F^y_\varphi(q)\frac{\partial q}{\partial y} = 0. \tag{9}$$

Hence, one infers from Eq. (7) that $F_\varphi$ is an entropy flux if and only if

$$\mathbf{D}\varphi(q)\mathbf{D}F^x(q) = \mathbf{D}F^x_\varphi(q), \quad \mathbf{D}\varphi(q)\mathbf{D}F^y(q) = \mathbf{D}F^y_\varphi(q). \tag{10}$$

The most prominant example of a generalized entropy is the thermodynamic entropy density $\varphi = \rho s$ together with the entropy flux $F_\varphi = \rho s U$, see, e.g. [23]. In this work, we will consider the thermodynamic entropy only, although many arguments below will carry over to generalized

entropies.

Differentiation of the condition for $F_\varphi$ to form an entropy flux (Eq. (10)) yields

$$\mathbf{D}^2\varphi(q)[\mathbf{D}F^x(q).,.] + \mathbf{D}\varphi(q)\mathbf{D}^2F^x(q)[.,.] = \mathbf{D}^2F^x_\varphi(q)[.,.], \tag{11}$$

with analogous formulas for the flux Jacobians in the other directions. Eq. (11) shows that its first summand is again symmetric, since the second one and the right-hand side are. Since $\varphi$ is strictly concave,

$$\langle u, v\rangle_\varphi = -\mathbf{D}^2\varphi(q)[u, v]$$

defines, for any $q$, an inner product. Note that this inner product depends, in the same way as a Riemannian metric[1], on the base state $q$. Restating the above, the flux Jacobians are symmetric with respect to this inner product, i.e.,

$$\langle \mathbf{D}F^x(q)[v], w\rangle_\varphi = \langle v, \mathbf{D}F^x(q)[w]\rangle_\varphi,$$

with analogous formulas for $\mathbf{D}F^y$ and $\mathbf{D}F^z$.

Consider the flow solution along a blade row interface at a certain radial height. For simplicity, we assume that the machine is axial and the interface is located at a constant axial position $x$ and radius $r$. Time-periodic flows can be decomposed into a temporal and circumferential average $\overline{q}^{\mathrm{a}}$ as well as a fluctuation $q'$,

$$q(t, x, r, \theta) = \overline{q}^{\mathrm{a}}(x, r) + q'(t, x, r, \theta).$$

[1] In fact, the Riemannian metric gives rise to a geometry that is closely related to the so-called *Ruppeiner geometry* [24].

Here, $\overline{q}^{\mathrm{a}}$ denotes the area average of $q$. The mixing entropy is defined as the difference between the entropy of the flux average and the mass-averaged entropy. The corresponding mixing entropy flux can be defined analogously as

$$\Delta F_{\varphi,\mathrm{mix}} = F^x_\varphi(\overline{q}^F) - \overline{F^x_\varphi(q)}^{\mathrm{a}}, \tag{12}$$

where $\overline{q}^F$ denotes the flux average. The mixing entropy is

$$\Delta s^F = \frac{\Delta F_{\varphi,\mathrm{mix}}}{\overline{\rho u}^{\mathrm{a}}},$$

where $u$ is the normal velocity [16].

We assume that the mean normal velocity is subsonic and non-vanishing which implies that $\mathbf{D}F^x(\overline{q}^{\mathrm{a}})$ is invertible. By definition, the flux average is a flow state $\overline{q}^F$ that satisfies

$$F^x(\overline{q}^F) = \overline{F^x(q)}^{\mathrm{a}}.$$

For sufficiently small disturbances, the normally subsonic flux average is uniquely defined. The second order Taylor expansion yields

$$\begin{aligned}
\overline{F^x(q)}^{\mathrm{a}} &= F^x(\overline{q}^{\mathrm{a}}) + \overline{\mathbf{D}F^x(\overline{q}^{\mathrm{a}})q'}^{\mathrm{a}} + \frac{1}{2}\overline{\mathbf{D}^2F^x(\overline{q}^{\mathrm{a}})[q',q']}^{\mathrm{a}} + \mathrm{O}(\|q'\|^3) \\
&= F^x(\overline{q}^{\mathrm{a}}) + \mathbf{D}F^x(\overline{q}^{\mathrm{a}})\overline{q'}^{\mathrm{a}} + \frac{1}{2}\overline{\mathbf{D}^2F^x(\overline{q}^{\mathrm{a}})[q',q']}^{\mathrm{a}} + \mathrm{O}(\|q'\|^3) \\
&= F^x(\overline{q}^{\mathrm{a}}) + \frac{1}{2}\overline{\mathbf{D}^2F^x(\overline{q}^{\mathrm{a}})[q',q']}^{\mathrm{a}} + \mathrm{O}(\|q'\|^3),
\end{aligned} \tag{13}$$

and thus, using the first-order Taylor expansion of $(F^x)^{-1}$ at $\overline{q}^{\mathrm{a}}$,

$$\overline{q}^F = \overline{q}^{\mathrm{a}} + \frac{1}{2}(\mathbf{D}F^x(\overline{q}^{\mathrm{a}}))^{-1}\overline{\mathbf{D}^2F^x(\overline{q}^{\mathrm{a}})[q',q']}^{\mathrm{a}} + \mathrm{O}(\|q'\|^3). \tag{14}$$

This implies that the entropy flux of the flux average (the first term on the right-hand side of (12)) can be approximated by

$$\begin{aligned} F^x_\varphi(\overline{q}^F) &= F^x_\varphi(\overline{q}^{\mathrm{a}}) + \frac{1}{2}\mathbf{D}F^x_\varphi(\overline{q}^{\mathrm{a}})\,(\mathbf{D}F^x(\overline{q}^{\mathrm{a}}))^{-1}\,\overline{\mathbf{D}^2F^x(\overline{q})[q',q']}^{\mathrm{a}} + \mathrm{O}(\|q'\|^3) \\ &= F^x_\varphi(\overline{q}^{\mathrm{a}}) + \frac{1}{2}\mathbf{D}\varphi(\overline{q}^{\mathrm{a}})\overline{\mathbf{D}^2F^x(\overline{q})[q',q']}^{\mathrm{a}} + \mathrm{O}(\|q'\|^3), \end{aligned} \tag{15}$$

where we have used (10). The equivalent statement as in (13) for $F^x_\varphi$ instead of $F^x$ is

$$\overline{F^x_\varphi(q)}^{\mathrm{a}} = F^x_\varphi(\overline{q}^{\mathrm{a}}) + \frac{1}{2}\overline{\mathbf{D}^2F^x_\varphi(\overline{q}^{\mathrm{a}})[q',q']}^{\mathrm{a}} + \mathrm{O}(\|q'\|^3). \tag{16}$$

Now, subtracting (16) from (15) gives the following approximation for the mixing entropy flux

$$\Delta F_{\varphi,\mathrm{mix}} = -\frac{1}{2}\overline{\mathbf{D}^2\varphi(\overline{q}^{\mathrm{a}})[\mathbf{D}F^x(\overline{q}^{\mathrm{a}})q',q']}^{\mathrm{a}} + \mathrm{O}(\|q'\|^3), \tag{17}$$

where we have used (11). Using the $L^2$-scalar product that corresponds to the inner product given by the entropy density Hessian,

$$\langle u',v'\rangle_{\varphi,L^2} = -\overline{\mathbf{D}^2\varphi(\overline{q}^{\mathrm{a}})[u',v']}^{\mathrm{a}}$$

the main result of this section reads as follows. The mixing entropy flux is approximated up to third

order by

$$\widetilde{\Delta F}_{\varphi,\mathrm{mix}} = \frac{1}{2}\big\langle \mathbf{D}F^x(\overline{q}^{\mathrm{a}})q' \,,\, q' \big\rangle_{\varphi,L^2}. \tag{18}$$

In the following, consider the 2D-Euler equations along the cylinder at radius $r$ and introduce the coordinate $y = r\theta$. For each complex vector $\mathbf{r}$ we consider plane waves

$$q' = \mathrm{Re}\left[\mathbf{r}e^{\mathbf{i}(\omega t+\xi x+\eta y)}\right] \tag{19}$$

with wave numbers $\xi$ and $\eta$ where $m = \eta r$ is the circumferential mode order. Whenever the angular frequencies or mode orders are different for two such waves $q'_1$, $q'_2$, the $L^2$-scalar product vanishes,

$$\big\langle q'_1 \,,\, q'_2 \big\rangle_{\varphi,L^2} = 0,$$

because of the $L^2$-orthogonality of trigonometric functions with different frequencies or wave numbers. For two waves $q'_1$, $q'_2$ with identical angular frequency $\omega = 2\pi/\Delta t$ and wave number $\eta = 2\pi/\Delta y$, we have

$$\begin{aligned}\big\langle q'_1 \,,\, q'_2 \big\rangle_{\varphi,L^2} &= \frac{1}{4\Delta t\Delta y}\int_0^{\Delta t}\int_0^{\Delta y} \mathbf{D}^2\varphi(\overline{q}^{\mathrm{a}})\Big[\mathbf{r}_1 e^{\mathbf{i}(\omega t+\eta y)} + \overline{\mathbf{r}_1}e^{-\mathbf{i}(\omega t+\eta y)}, \mathbf{r}_2 e^{\mathbf{i}(\omega t+\eta y)} + \overline{\mathbf{r}_2}e^{-\mathbf{i}(\omega t+\eta y)}\Big]\,dydt \\ &= \frac{1}{2}\,\mathrm{Re}\,\big\langle \mathbf{r}_1 \,,\, \mathbf{r}_2 \big\rangle_{\varphi}.\end{aligned} \tag{20}$$

where the scalar product is generalized to complex vectors such that it is anti-linear in the first component.

If a general disturbance $q'$ with angular frequency $\omega$ and tangential wave number $\eta$ is given as

a sum of fundamental waves of the form (19),

$$q' = \sum_j \mathrm{Re}\left[\mathbf{r}^{(j)} e^{\mathbf{i}(\omega t + \xi_j x + \eta y)}\right],$$

then (18) and (20) imply

$$\widetilde{\Delta F}_{\varphi,\mathrm{mix}} = \frac{1}{4}\sum_{j_1,j_2} \mathrm{Re}\left\langle \mathbf{D}F^x(\overline{q}^{\mathrm{a}})\mathbf{r}^{(j_1)}\,,\,\mathbf{r}^{(j_2)}\right\rangle_{\varphi}. \tag{21}$$

The next step is to evaluate the inner products in (21) for plane wave solutions, i.e., for vectors $\mathbf{r}$ which are solutions to the dispersion relation

$$\left(\omega + \xi\mathbf{D}F^x + \eta\mathbf{D}F^y\right)\mathbf{r} = 0, \tag{22}$$

i.e., right-eigenvectors $\mathbf{r}$, such that the corresponding $q'$ is a solution to the Euler equations, linearized at the average state $\overline{q}^{\mathrm{a}}$,

$$\frac{\partial q'}{\partial t} + \mathbf{D}F^x\frac{\partial q'}{\partial x} + \mathbf{D}F^y\frac{\partial q'}{\partial y} = 0.$$

Here, to keep the notation simple, we have dropped the explicit dependency of the Jacobians on $\overline{q}^{\mathrm{a}}$.

Consider two right-eigenvectors $\mathbf{r}_1$ and $\mathbf{r}_2$ which belong to a single tangential wave number $\eta$ and possibly different angular frequencies $\omega_{1/2} \in \mathbb{R}_{\geq 0}$ and normal wave numbers $\xi_{1/2} \in \mathbb{C}$. Making

use of the symmetry of the flux Jacobians with respect to the inner product $\langle .\,,\,. \rangle$, one deduces

$$\begin{aligned}(\overline{\xi_1} - \xi_2)\big\langle \mathbf{D}F^x\mathbf{r}_1\,,\,\mathbf{r}_2\big\rangle_\varphi &= \big\langle \xi_1\mathbf{D}F^x\mathbf{r}_1\,,\,\mathbf{r}_2\big\rangle_\varphi - \big\langle \mathbf{r}_1\,,\,\xi_2\mathbf{D}F^x\mathbf{r}_2\big\rangle_\varphi \\ &= -\big\langle (\omega_1 + \eta\mathbf{D}F^y)\mathbf{r}_1\,,\,\mathbf{r}_2\big\rangle_\varphi \\ &\quad + \big\langle \mathbf{r}_1\,,\,(\omega_2 + \eta\mathbf{D}F^y)\mathbf{r}_2\big\rangle_\varphi \\ &= -(\omega_1 - \omega_2)\big\langle \mathbf{r}_1\,,\,\mathbf{r}_2\big\rangle_\varphi.\end{aligned} \tag{23}$$

Hence, if $\xi_1 \neq \overline{\xi_2}$, then

$$\big\langle \mathbf{D}F^x\mathbf{r}_1\,,\,\mathbf{r}_2\big\rangle_\varphi = -\frac{\omega_1 - \omega_2}{\overline{\xi_1} - \xi_2}\big\langle \mathbf{r}_1\,,\,\mathbf{r}_2\big\rangle_\varphi. \tag{24}$$

This shows that the right eigenvectors of modes whose frequencies and circumferential wavenumbers are identical, but whose axial wavenumbers are not complex conjugates of each other, must satisfy

$$\big\langle \mathbf{D}F^x\mathbf{r}_1\,,\,\mathbf{r}_2\big\rangle_\varphi = 0,$$

so the cross-coupling terms between these modes vanish. In particular, convective as well as left- and right-running acoustic cut-on modes yield separate contributions to the second-order approximation of mixing entropy. For these modes, the normal wave number $\xi$ is real. Moreover, unless acoustic resonance occurs, $\omega$ and $r$ depend differentiably on $\xi$ [25]. So taking the limit $\xi_2 \to \xi_1$ in Eq. (24) for a family of corresponding eigenvectors yields

$$\big\langle \mathbf{D}F^x\mathbf{r}\,,\,\mathbf{r}\big\rangle_\varphi = u_\mathrm{g} \cdot \langle \mathbf{r}, \mathbf{r}\rangle_\varphi. \tag{25}$$

where $u_\mathrm{g}$ denotes the axial group velocity, which, with our sign convention, is $-\frac{\partial\omega}{\partial\xi}$.

For cut-off acoustic modes, the last line of (23) tends to zero for $\xi_2 \to \xi_1$ whereas $\overline{\xi_1} - \xi_2$ converges to $-2\mathbf{i}\,\mathrm{Im}\,\xi_1 \neq 0$, which implies that

$$\left\langle \mathbf{D}F^x\mathbf{r}\,,\,\mathbf{r}\right\rangle_\varphi = 0$$

for cut-off modes. Expressing $\left\langle \mathbf{D}F^x\mathbf{r}_1\,,\,\mathbf{r}_2\right\rangle_\varphi$ in a modal basis would thus yield zero diagonal terms for cut-off acoustic modes. On the other hand, the axial wavenumbers as well as the right-eigenvectors of the up- and downstream running cut-off modes are complex conjugates of each other, so the off-diagonal terms contain expressions of the form

$$\left\langle \mathbf{D}F^x\mathbf{r}\,,\,\overline{\mathbf{r}}\right\rangle_\varphi$$

with cut-off acoustic eigenvectors $\mathbf{r}$ and $\overline{\mathbf{r}}$. Note that these cross-coupling terms are non-zero and may represent a significant contribution to the overall mixing entropy at blade row interfaces where both up- and downstream disturbances exist [15].

### Relation to Sound Intensity

To evaluate the second-order mixing entropy (25) for acoustic modes, we will use the following expression for the Hessian of the entropy density w.r.t. the conservative variables, but expressed in terms of primitive disturbances,

$$\begin{aligned}\langle q_1', q_2'\rangle_\varphi &= -\mathbf{D}^2(\rho s)[q_1', q_2'] = -(q_1')^\mathrm{H}\frac{\partial^2(\rho s)}{\partial q^2}{q_2}' \\ &= c_\mathrm{v}\rho \begin{pmatrix} \rho_1'/\rho \\ U_1'/a \\ p_1'/p \end{pmatrix}^\mathrm{H} \begin{pmatrix} \gamma & 0 & -1 \\ 0 & \gamma(\gamma-1) & 0 \\ -1 & 0 & 1 \end{pmatrix} \begin{pmatrix} \rho_2'/\rho \\ U_2'/a \\ p_2'/p \end{pmatrix}.\end{aligned} \tag{26}$$

see [15]. Here, and in the following, we simply write $\rho$, $p$,... for the averaged variables $\overline{\rho}^{\mathrm{a}}$, $\overline{p}^{\mathrm{a}}$ etc. For

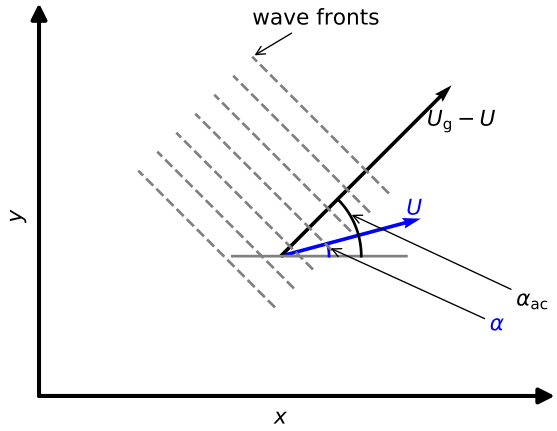


Fig. 1: Flow angle $\alpha$ and inclination angle of wave fronts $\alpha_{\mathrm{ac}}$.

a 2D acoustic mode with angular frequency $\omega$ and wave numbers $\xi, \eta$, the primitive disturbances are given by (cf. [26])

$$q'_{\mathrm{p}} = \mathrm{Re}\left[\frac{\hat{p}_\omega}{\gamma p}\begin{pmatrix}\rho\\ -\frac{a^2\xi}{\omega+\xi u+\eta v}\\ -\frac{a^2\eta}{\omega+\xi u+\eta v}\\ \gamma p\end{pmatrix} e^{\mathbf{i}(\omega t+\xi_j x+\eta y)}\right].$$

Here $\omega, \xi, \eta$ satisfy the dispersion relation

$$(\omega + \xi u + \eta v)^2 = a^2(\xi^2 + \eta^2). \tag{27}$$

Hence, the mixing entropy flux due to a single acoustic mode is

$$\begin{aligned}\widetilde{\Delta F}_{\varphi,\mathrm{mix}} &= \frac{1}{4}\sum_{j_1,j_2}\mathrm{Re}\left\langle \mathbf{D}F^x(\overline{q}^{\mathrm{a}})q'\,,\,q'\right\rangle_{\varphi}\\ &= \frac{u_{\mathrm{g}}}{4}\left\langle q'\,,\,q'\right\rangle_{\varphi}\\ &= \frac{u_{\mathrm{g}}}{4}\rho c_{\mathrm{v}}(\gamma-2\gamma+\gamma(\gamma-1)+\gamma^2)\left|\frac{\hat{p}_\omega}{\gamma p}\right|^2\\ &= \frac{\rho c_{\mathrm{v}}(\gamma-1)}{2\gamma}u_{\mathrm{g}}\left|\frac{\hat{p}_\omega}{p}\right|^2.\end{aligned} \tag{28}$$

Let us denote the time-average of quantity $q$ by $\overline{q}^t$. The axial sound intensity is given by (cf. [27])

$$\begin{aligned}I_x &= \overline{\left(\frac{\rho'}{\rho}u+u'\right)(p'+\rho U\cdot U')}^t\\ &= \frac{1}{2}\left|\frac{\hat{p}_\omega}{\gamma p}\right|^2\left(u-\frac{a^2\xi}{\omega+\xi u+\eta v}\right)(\gamma p+\rho U\cdot(U_{\mathrm{g}}-U))\\ &= \frac{\rho a^2}{2\gamma^2}\left|\frac{\hat{p}_\omega}{p}\right|^2 u_{\mathrm{g}}\left(1+\frac{U\cdot(U_{\mathrm{g}}-U)}{a^2}\right)\\ &= \frac{\rho c_{\mathrm{v}}(\gamma-1)T}{2\gamma}u_{\mathrm{g}}\left|\frac{\hat{p}_\omega}{p}\right|^2\left(1+\frac{U\cdot(U_{\mathrm{g}}-U)}{a^2}\right)\end{aligned} \tag{29}$$

where we have used that, by (27), the group velocity of the acoustic wave is

$$U_{\mathrm{g}}=\begin{pmatrix}u_{\mathrm{g}}\\ v_{\mathrm{g}}\end{pmatrix},\quad u_{\mathrm{g}}=u-\frac{a^2\xi}{\omega+\xi u+\eta v},\quad v_{\mathrm{g}}=v-\frac{a^2\eta}{\omega+\xi u+\eta v},$$

so

$$\hat{U}=\frac{\hat{p}}{\gamma p}(U_{\mathrm{g}}-U).$$

It follows that the sound intensity (29) differs from the second-order approximation of the mixing entropy flux (28) by a factor of

$$\left(1 + \frac{U \cdot (U_\mathrm{g} - U)}{a^2}\right) T = (1 + M\cos(\alpha - \alpha_\mathrm{ac}))T$$

where the flow angle $\alpha$ and the inclination $\alpha_\mathrm{ac}$ of the acoustic wave fronts are as depicted in Fig. 1. In particular, in a fluid at rest, sound power is the product of the second-order approximated integrated mixing entropy flux and the temperature.

## APPLICATION

We study the problem of selecting the harmonics for an HB simulation of the first stator and the second stage of DLR's 4.5 stage transonic research compressor Rig 250, cf. [28]. All simulations discussed here were performed on the same mesh which, at 50% channel height, is depicted in Fig. 2. The boundary conditions correspond to the aerodynamic design point. The flow regime in Rotor 2 is transonic with relative tip Mach numbers of about 1.45. The harmonic balance approach was applied both to the flow and turbulence equations, i.e., in contrast to the results shown in [10], no 'frozen turbulence' assumption was used.

| Blade Row | # Blades | $\Omega$ | # Grid points |
|---|---|---|---|
| Stator 1 | 36 | 0 | 1 004 571 |
| Rotor 2 | 28 | -2$\pi\cdot$ 216 Hz | 882 763 |
| Stator 2 | 48 | 0 | 1 014 178 |

Table 1: Blade row configuration

We concentrate here on the question of relevant harmonics in the second stator. It can be seen from the blade counts for the three rows (see Tab. 1) that if the computational domain comprises four passages of the Stator 2 row, then the flow in that row is periodic with the blade passing frequency of Rotor 2, denoted by $\mathrm{BPF}_2$, and a single phase-lag at the periodic boundaries of the

resulting one-twelfth annulus. In contrast, if the domain consists of a single passage in Stator 2, then four harmonics with frequency $\mathrm{BPF}_2$ but different interblade phase angles are generated by the interaction with Stator 1.

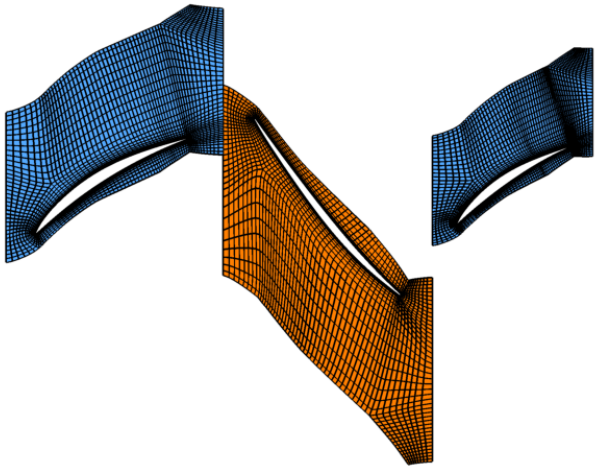

Fig. 2: Mesh (every second grid line) at midspan for Stator 1, Rotor 2, and Stator 2.

To explain this in detail, the disturbances due to Stator 1 and Rotor 2 are superpositions of modes of the form

$$\mathrm{Re}\left[\hat{q}e^{\mathbf{i}(28k|\Omega|t+(28k+36l)\theta)}\right].$$

Here, $28|\Omega| = 2\pi\mathrm{BPF}_2$ is the blade passing (angular) frequency of Rotor 2, $k$ is the harmonic index and $l$ will be called the *scatter index*. Note that the modes corresponding to $l = 0$ are those that would be taken into account, if the stator-stator interaction were neglected. It follows that the $k$-th harmonic in Stator 2 will contain modes with different interblade phase angles given by

$$\sigma_{k,l} \equiv 2\pi\left(-\frac{5k}{12} - \frac{l}{4}\right) \mod 2\pi.$$

Observe that scattering indices which differ by a multiple of $4$ correspond to the same interblade phase angle. The resulting first harmonics in Stator 2 are summarized in Tab. 2.

First, a standard harmonic balance setup which resolves the influence of neighboring rows with three harmonics is simulated, see Tab. 3. The solver is initialized with a steady flow solution. Although this simulation does not resolve any stator-stator interaction, the modes that result from the interaction between Stator 1 and Rotor 2 which would give rise to the above-mentioned scattered modes, are visible at the rotor outlet. The last line in Tab. 2 shows the mode orders that correspond to the first harmonic in Stator 2 ($k = 1$) and the given scatter index $l$ with maximal mixing entropy at the rotor outlet. Note that the sign of the mode order refers to the stator frame of reference. Figure 3 shows the convergence of the mixing entropies of these mode orders $m_{\max}$ for each scattering index $l = -1, +1, -2$. Here, the radial distribution of mixing entropies is mass averaged to obtain an integral value. As can be seen in the plot, the mixing entropies are nearly zero for some time, since it takes a certain number of pseudo-time steps to propagate the disturbances to the rotor outlet. Figure 3 shows little qualitative difference for those modes whose

| $l$ | 0 | -1 | +1 | -2 |
|---|---|---|---|---|
| $\sigma_{1,l}$ | -150deg | -60deg | +120deg | +30deg |
| $m_{\max}$ | +28 | -8 | +64 | -44 |

Table 2: Harmonics in Stator 2, single passage

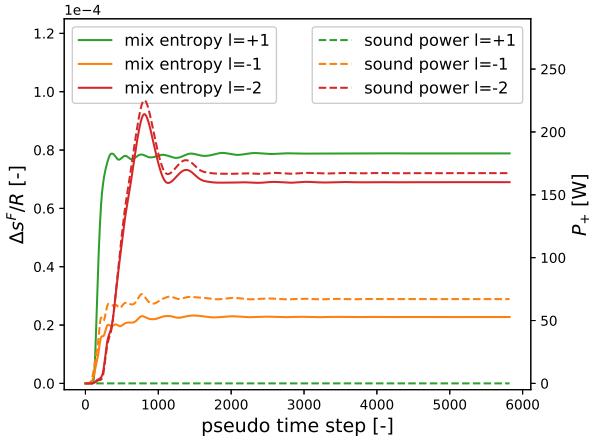


Fig. 3: Mixing entropy and sound power attributed to Tyler-Sofrin modes.

| Blade row | Frequency | Harmonics |
|---|---|---|
| Stator 1 | $\mathrm{BPF}_2$ | 0-3 |
| Rotor 2 | $\mathrm{VPF}_1$ | 0-3 |
| Rotor 2 | $\mathrm{VPF}_2$ | 0-3 |
| Sator 2 | $\mathrm{BPF}_2$ | 0-3 |

Table 3: Standard setup

acoustic component is cut-on ($l = -1, -2$). For $l = +1$, however, all acoustic modes are cut-off. Here, mixing entropy represents a physically meaningful measure on which convergence criteria can be based.

Figure 4 shows the mixing entropies of the converged solution for each mode type, i.e., entropy, vorticity and downstream acoustic modes, at the rotor outlet. We have used, at each radius, a 2D wave splitting, i.e., the disturbances are decomposed into families of eigenvectors of the dispersion relation (Eq. (22)). Here, the sum over all modes that belong to the same scatter index are shown, so different colors correspond to different interblade phase angles in Stator 2. The interblade phase angles for the harmonic sets in Stator 2 are as in Tab. 2. Each column represents the contributions to one harmonic in the second stator. In particular, the first columns correspond to so-called clocking modes, i.e., vane-to-vane asymmetries of the mean flow which, in a single-passage configuration, cannot be resolved with the standard harmonic balance approach.

Then a harmonic balance simulation is performed with harmonic sets as listed in Tab. 4. Here, seven harmonics are used to resolve the interaction with the neighboring row. Moreover, we add harmonic sets to resolve the vane-to-vane asymmetry of the mean flow and first harmonic in Stator 2. To quantify the impact of the additional harmonic sets for the first vane pressure harmonic in Stator 2, Fig. 5b) shows the root mean squared amplitude of the first pressure harmonic on the vane surfaces of Stator 2, where the *mean* refers to an area average over the whole vane surface. One can see that the Tyler-Sofrin modes have a considerable impact on the pressure harmonics and their sum is in the same order of magnitude as the harmonics due to Rotor 2 only ($l = 0$). In Fig. 5a), the total amount of mixing entropy of the previous harmonic balance

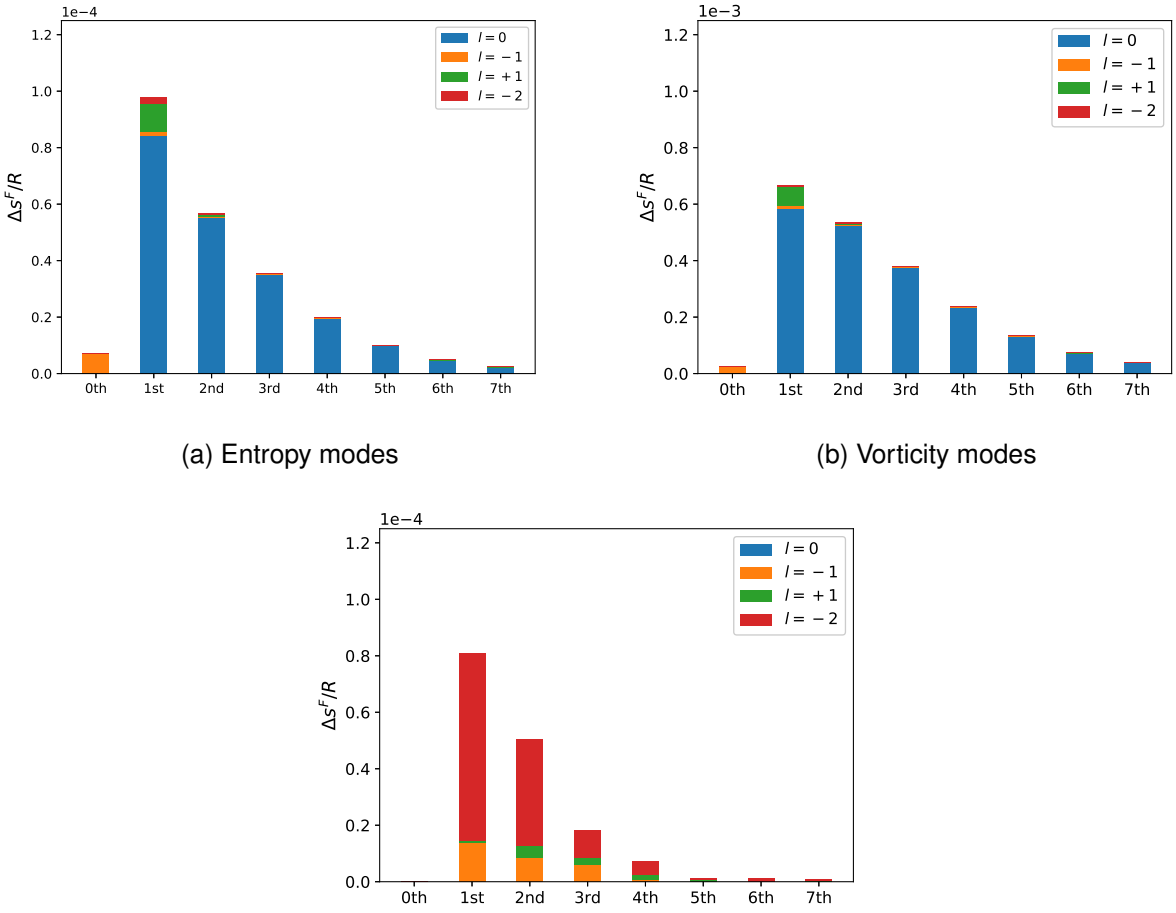


(a) Entropy modes

(b) Vorticity modes

(c) Acoustic modes

Fig. 4: Mixing entropies at outlet of Rotor 2 for higher harmonics and different scatter indices.

setup is shown for comparison. It turns out, that although the mixing entropy analysis predicted a significant impact of the Tyler-Sofrin modes, the impact on the vane pressure harmonics does not scale with the mixing entropy (or its square root, the mixing entropy scales with the square of the amplitudes). It rather seems that, in order to predict the impact a particular scatter index has on unsteady pressures, the mode type which contributes most to the mixing entropy should be taken into account. In our example, the green block ($l = +1$) is almost entirely due to vorticity modes, as the corresponding acoustic disturbances are cut-off. The Tyler-Sofrin vorticity modes seem to affect the vane pressure harmonics but to a somewhat lesser extent than, for instance the $l = -2$ modes, whose overall mixing entropy is comparable to $l = +1$, but which contain a cut-on acoustic

| Blade row | Frequency | Scatter index | Harmonics |
|---|---|---|---|
| Stator 1 | $\mathrm{BPF}_2$ | 0 | 0-7 |
| Rotor 2 | $\mathrm{VPF}_1$ | 0 | 0-7 |
| Rotor 2 | $\mathrm{VPF}_2$ | 0 | 0-7 |
| Stator 2 | $\mathrm{BPF}_2$ | 0 | 0-7 |
| Stator 2 | $\mathrm{BPF}_2$ | -1 | 0-1 |
| Stator 2 | $\mathrm{BPF}_2$ | +1 | 0-1 |
| Stator 2 | $\mathrm{BPF}_2$ | -2 | 0-1 |
| Stator 2 | $0$ | 1 | 0-3 |

Table 4: Setup using harmonic sets

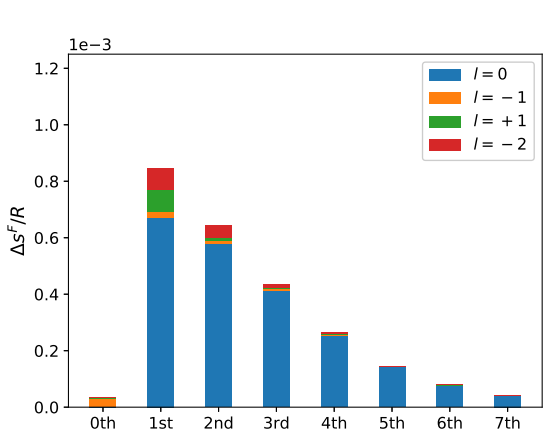


(a) Mixing entropies

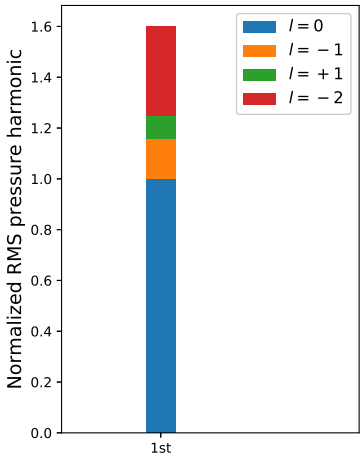


(b) Vane pressure harmonics (RMS)

Fig. 5: Mixing entropies at Rotor 2 outlet predicted with the standard setup and first pressure harmonics on vane surfaces of Stator 2 resulting from the simulation with additional harmonic sets for Tyler-Sofrin modes.

mode.

The harmonic set approach is based on the simplifying assumption that the nonlinear interaction between two harmonic sets is solely due to common harmonics, e.g., through the time-mean flow [10, 11]. For comparison, a simulation with four passages in the second stator was performed. The harmonic balance setup is summarized in Table 5. Figures 6 and 7 compare the harmonic

set to the multi-passage approach in terms of the first pressure harmonics on a sector of four vanes of Stator 2. The agreement between the two approaches is high, so we conclude that both the nonlinear interaction between the harmonics corresponding to different scatter indices and the nonlinear influence of the so-called *clocking* harmonic on the first harmonic is, in our configuration, negligible. Moreover, the vane-to-vane variation of the amplitudes shows the strong impact of the Tyler-Sofrin modes on the pressure harmonics. It is thus indispensable to include scattered harmonics in order to predict accurate unsteady pressures, either through multi-passage configurations or approaches which allow for multiple interblade phase angles.

## CONCLUSIONS

In this paper, the second-order mixing entropy attributed to different temporal and circumferential Fourier modes is studied and its significance for the analysis of harmonic balance results is highlighted. Harmonic balance results of multi-stage turbomachinery configurations with a reasonably low number of harmonics contain several types of errors that, in practical applications, should be estimated. Being a Fourier-Galerkin approach, harmonic balance methods naturally produce truncation and aliasing errors whose order of magnitude can be quantified in harmonic convergence studies. The presence of a huge number of Tyler-Sofrin modes, however, requires a systematic approach to estimate the impact that the mixing out of certain modes at the blade row interfaces has. For this problem, mixing entropy can serve as a physically meaningful quantity. Our results show, however, that the impact on surface pressure harmonics does not simply scale with the mixing entropy. The authors suggest that the mode type should be taken into account in

| Blade row | Frequency | # Passages | Harmonics |
|---|---|---|---|
| Stator 1 | $\mathrm{BPF}_2$ | 1 | 0-7 |
| Rotor 2 | $\mathrm{VPF}_1$ | 1 | 0-7 |
| Rotor 2 | $\mathrm{VPF}_2$ | 1 | 0-7 |
| Stator 2 | $\mathrm{BPF}_2$ | 4 | 0-7 |

Table 5: Setup using multiple passages in Stator 2

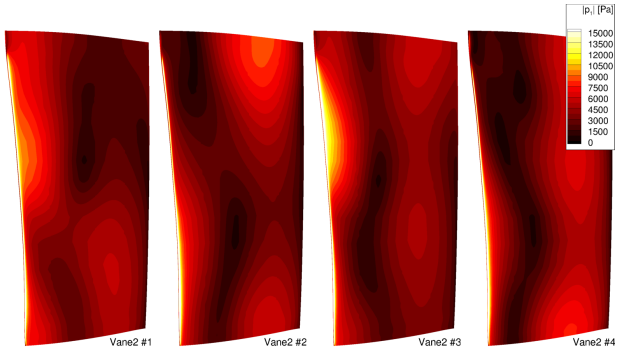


(a) Multi-passage

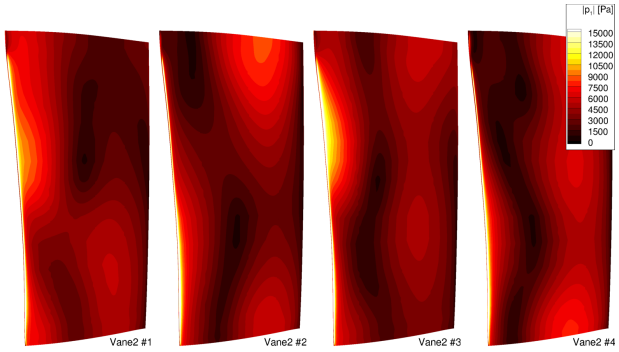


(b) Harmonic sets

Fig. 6: Amplitude of first pressure harmonics on pressure sides of Stator 2.

order to decide which scatter index is the most important one. In particular, if the modal analysis points to the presence of relevant Tyler-Sofrin cut-on acoustic modes, the corresponding scatter index should be resolved even if the corresponding mixing entropy is somewhat smaller than that of another purely vortical mode. For such a distinction, the fact that the mixing entropy of a mode order can be further decomposed into acoustic, vorticity and entropy modes seems useful.

The application of the harmonic balance approach to a three-blade row compressor configuration pointed to the importance of including Tyler-Sofrin modes in the harmonic balance approaches. The results show a very good agreement of the harmonic-set and multi-passage results.

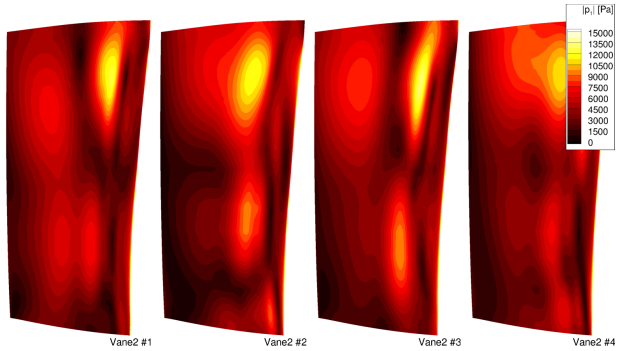


(a) Multi-passage

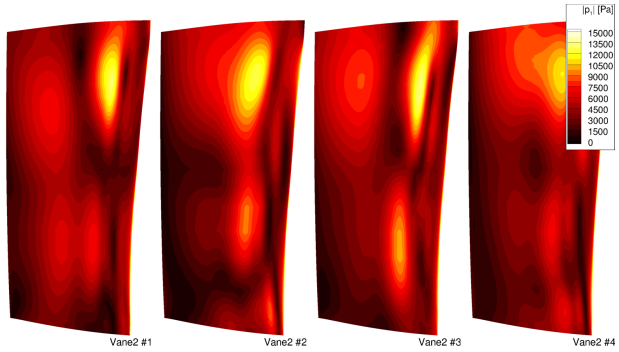


(b) Harmonic sets

Fig. 7: Amplitude of first pressure harmonics on suction sides of Stator 2.


## ACKNOWLEDGEMENTS

The authors acknowledge the financial support by the Federal Ministry for Economic Affairs and Climate Action of Germany in the framework of the joint project ROBOFLEX (grant number 03EE5013P) which is part of the research corporation *AG Turbo*. The authors would also like to express their gratitude to Siemens Energy for co-financing this project.


## NOMENCLATURE

### Latin symbols

$a$ speed of sound

$c_\mathrm{v}$ specific heat capacity at constant volume

$\mathbf{i}$ square root of $-1$

$k$ harmonic index

$l$ scatter index

m circumferential mode order

$p$ pressure

$q$ vector of conservative variables

$q_{\mathrm{p}}$ vector of primitive variables

$\hat{q}$ Fourier coefficient of $q$

$\overline{q}^a$ area average of $q$

$\overline{q}^F$ flux average of $q$

$q'$ disturbance of $q$

$\mathbf{r}$ right eigenvector of dispersion relation

$s$ entropy

$v^{\mathrm{H}}$ hermitian transpose of complex vector $v$

$u, v$ velocity components

$u_{\mathrm{g}}$ $x$-component of group velocity

$x, y$ Cartesian coordinates

$x, r, \theta$ cylindrical coordinates

$\mathrm{Re}\, z, \mathrm{Im}\, z$ real and imaginary parts of $z$

$\overline{z}$ complex conjugate of $z$

$\mathbf{D}F$ Jacobian of $F$

$F$ Euler flux

$F_\varphi$ entropy flux

$\Delta F_{\varphi,\mathrm{mix}}$ mixing entropy flux

$\widetilde{\Delta F}_{\varphi,\mathrm{mix}}$ second order approximation of $\Delta F_{\varphi,\mathrm{mix}}$

$\Delta s^F$ mixing entropy

$M$ Mach number

$R$ specific gas constant

$R(q)$ flow residual

$\mathscr{S}$ harmonic set

$T$ temperature

$U$ velocity

**Greek symbols**

$\alpha$ flow angle

$\alpha_{\mathrm{ac}}$ wave front angle

$\varphi$ entropy density

$\rho$ density

$\sigma$ interblade phase angle value

$\xi, \eta$ $x$- and $y$-wave numbers

$\omega$ angular frequency

$\Omega$ Rotational speed

**Abbreviations**

$\mathrm{BPF}_i$ blade passing frequency of the $i$-th rotor

$\mathrm{VPF}_i$ vane passing frequency of the $i$-th stator

**REFERENCES**


[1] Li, H. D., and He, L., 2003, "Blade count and clocking effects on three-bladerow interaction in a transonic turbine," *J. Turbomach.,* **125**(4), Dec., pp. 632–640.

[2] Hall, K. C., and Ekici, K., 2005, "Multistage coupling for unsteady flows in turbomachinery," *AIAA J.,* **43**(3), Mar., pp. 624–632.

[3] Schoenenborn, H., and Ashcroft, G., 2014, "Comparison of non-linear and linearized CFD analysis of the stator-rotor interaction of a compressor stage," In Proceedings of ASME Turbo Expo 2014.

[4] Li, H. D., and He, L., 2005, "Blade aerodynamic damping variation with rotor-stator gap: A computational study using single-passage approach," *J. Turbomach,* **127**(3), pp. 573–579.

[5] Rahmati, M., He, L., and Sheng, Y., 2012, "Multi-row interference effects on blade aeromechanics in compressor and turbine stages," In 13th International Symposium on Unsteady

Aerodynamics, Aeroacoustics and Aeroelasticity of Turbomachines 2012 (ISUAAAT 13), Vol. 1.

[6] Kersken, H.-P., Frey, C., Ashcroft, G., and Schönenborn, H., 2017, "Flutter analysis of an embedded blade row with a harmonic balance solver," In Proceedings of 12th European Conference on Turbomachinery Fluid dynamics & Thermodynamics.

[7] Schoenenborn, H., 2018, "Analysis of the effect of multirow and multipassage aerodynamic interaction on the forced response variation in a compressor configuration–part i: Aerodynamic excitation," *J. Turbomach,* **140**(5), Feb.

[8] Guedeney, T., Gomar, A., Gallard, F., Sicot, F., Dufour, G., and Puigt, G., 2013, "Non-uniform time sampling for multiple-frequency harmonic balance computations," *J. Comput. Phys.,* **236**, pp. 317–345.

[9] Subramanian, V., Custer, C. H., Weiss, J. M., and Hall, K. C., 2013, "Unsteady simulation of a two-stage cooled high pressure turbine using an efficient non-linear harmonic balance method," In Proceedings of the ASME Turbo Expo 2013.

[10] Frey, C., Ashcroft, G., Kersken, H.-P., and Voigt, C., 2014, "A harmonic balance technique for multistage turbomachinery applications," In ASME Turbo Expo 2014: Turbine Technical Conference and Exposition, p. V02BT39A005.

[11] Frey, C., Ashcroft, G., Kersken, H.-P., Schönweitz, D., and Mennicken, M., 2018, "Simulation of indexing and clocking with harmonic balance," *Int. J. Turbomach. Propuls. Power,* **3**(1).

[12] Junge, L., Frey, C., Ashcroft, G., and Kuegeler, E., 2021, "A New Harmonic Balance Approach Using Multidimensional Time," *Journal of Engineering for Gas Turbines and Power*, 01.

[13] Fritsch, G., 1992, "An analytical and numerical study of the second-order effects of unsteadiness on the performance of turbomachines," PhD thesis, Massachusetts Institute of Technology, Cambridge, MA.

[14] Fritsch, G., and Giles, M. B., 1995, "An asymptotic analysis of mixing loss," *J. Turbomach.,* **117**, p. 367.

[15] Schlüß, D., and Frey, C., 2018, "Mixing Losses in Steady and Unsteady Simulations of Turbomachinery Flows," In ASME Turbo Expo: Power for Land, Sea, and Air, Vol. 2C,

p. V02CT42A014.

[16] Frey, C., Ashcroft, G., Müller, M., and Wellner, J., 2022, "Analysis of Turbomachinery Averaging Techniques," *Journal of Turbomachinery,* **145**(5) 051006.

[17] Roe, P. L., 1981, "Approximate Riemann solvers, parameter vectors, and difference schemes," *J. Comput. Phys.,* **43**(2), pp. 357 – 372.

[18] van Leer, B., 1979, "Towards the ultimate conservative difference scheme. V. A second-order sequel to Godunov's method," *J. Comput. Phys.,* **32**(1), pp. 101 – 136.

[19] van Albada, G. D., van Leer, B., and Roberts, Jr., W. W., 1982, "A comparative study of computational methods in cosmic gas dynamics," *Astron. Astrophys.,* **108**(1), pp. 76–84.

[20] Wilcox, D. C., 1988, "Reassessment of the scale-determining equation for advanced turbulence models," *AIAA J.,* **26**(11), pp. 1299–1310.

[21] Orszag, S. A., 1971, "Elimination of aliasing in finite-difference schemes by filtering high-wavenumber components," *J. Atmos. Sci.,* **28**, p. 1074.

[22] Frey, C., Ashcroft, G., and Kersken, H.-P., 2015, "Simulations of Unsteady Blade Row Interactions Using Linear and Non-Linear Frequency Domain Methods," In Turbo Expo: Power for Land, Sea, and Air, Vol. Volume 2B: Turbomachinery, p. V02BT39A037.

[23] Godlewski, E., and Raviart, P., 1996, *Numerical Approximation of Hyperbolic Systems of Conservation Laws* No. 118 in Applied Mathematical Sciences. Springer.

[24] Ruppeiner, G., 1979, "Thermodynamics: A Riemannian geometric model," *Phys. Rev. A,* **20**, Oct, pp. 1608–1613.

[25] Frey, C., and Kersken, H.-P., 2016, "On the regularisation of non-reflecting boundary conditions near acoustic resonance," In ECCOMAS Congress 2016 VII European Congress on Computational Methods in Applied Sciences and Engineering, Crete Island, Greece.

[26] Kersken, H.-P., Ashcroft, G., Frey, C., Wolfrum, N., and Korte, D., 2014, "Nonreflecting boundary conditions for aeroelastic analysis in time and frequency domain 3D RANS solvers," In Proceedings of ASME Turbo Expo 2014.

[27] Morfey, C., 1971, "Acoustic energy in non-uniform flows," *Journal of Sound and Vibration,* **14**(2), pp. 159 – 170.

[28] Röber, T., Kügeler, E., and Weber, A., 2010, “Investigation of unsteady flow effects in an axial compressor based on whole annulus computations,” In Proceedings of the ASME Turbo Expo 2010.

**LIST OF FIGURES**


1 Flow angle $\alpha$ and inclination angle of wave fronts $\alpha_{\mathrm{ac}}$. . . . . 17

2 Mesh (every second grid line) at midspan for Stator 1, Rotor 2, and Stator 2. . . . . 20

3 Mixing entropy and sound power attributed to Tyler-Sofrin modes. . . . . 21

4 Mixing entropies at outlet of Rotor 2 for higher harmonics and different scatter indices. 23

5 Mixing entropies at Rotor 2 outlet predicted with the standard setup and first pressure harmonics on vane surfaces of Stator 2 resulting from the simulation with additional harmonic sets for Tyler-Sofrin modes. . . . . 24

6 Amplitude of first pressure harmonics on pressure sides of Stator 2. . . . . 26

7 Amplitude of first pressure harmonics on suction sides of Stator 2. . . . . 27

## LIST OF TABLES


1 Blade row configuration . . . . . 19

2 Harmonics in Stator 2, single passage . . . . . 21

3 Standard setup . . . . . 22

4 Setup using harmonic sets . . . . . 24

5 Setup using multiple passages in Stator 2 . . . . . 25